




# Polarization of Gamma-Ray Bursts in the Dissipative Photosphere Model

Christoffer Lundman<sup>1,2,3</sup>, Indrek Vurm<sup>1,4</sup> , and Andrei M. Beloborodov<sup>1</sup>

<sup>1</sup> Physics Department and Columbia Astrophysics Laboratory, Columbia University, 538 West 120th Street, New York, NY 10027, USA; [clundman@particle.kth.se](mailto:clundman@particle.kth.se)

<sup>2</sup> Department of Physics, KTH Royal Institute of Technology, AlbaNova, SE-106 91 Stockholm, Sweden

<sup>3</sup> The Oskar Klein Centre for Cosmoparticle Physics, AlbaNova, SE-106 91 Stockholm, Sweden

<sup>4</sup> Tartu Observatory, Tõravere 61602, Tartumaa, Estonia

Received 2016 November 4; revised 2018 February 13; accepted 2018 March 2; published 2018 April 3

## Abstract

The MeV spectral peak of gamma-ray bursts (GRBs) is best explained as photospheric emission from a dissipative relativistic jet. The observed non-blackbody spectrum shows that sub-photospheric dissipation involves both thermal plasma heating and injection of nonthermal particles, which quickly cool through inverse Compton scattering and emission of synchrotron radiation. Synchrotron photons emitted around and above the photosphere are predicted to dominate the low-energy part of the GRB spectrum, starting from roughly a decade in energy below the MeV peak. We show that this leads to a unique polarization signature: a rise in GRB polarization toward lower energies. We compute the polarization degree of GRB radiation as a function of photon energy for a generic jet model, and show the predictions for GRBs 990123, 090902B, and 110721A. The expected polarization is significant in the X-ray band, in particular for bursts similar to GRB 090902B. The model predicts that radiation in the MeV peak (and at higher energies) is unpolarized as long as the jet is approximately uniform on angular scales  $\delta\theta \gtrsim \Gamma^{-1}$  where  $\Gamma$  is the bulk Lorentz factor of the jet.

**Key words:** gamma-ray burst: general – polarization – radiation mechanisms: non-thermal – radiative transfer – relativistic processes – scattering

## 1. Introduction

The polarization properties of gamma-ray bursts (GRBs) are poorly known, and future measurements are expected to provide important tests for the burst emission mechanism. Current polarization measurements<sup>5</sup> suffer from low photon statistics, although claims of detection of linear polarization degrees of a few tens percent have been made (Götz et al. 2009, 2013, 2014; Yonetoku et al. 2011, 2012).

Linear polarization is often viewed as a signature of synchrotron emission (e.g., Götz et al. 2009, 2013; Yonetoku et al. 2012; Deng et al. 2016). On the other hand, several characteristics of the GRB spectrum suggest that the observed MeV peak is not synchrotron radiation. First, the spectral indices below the main MeV peak are typically harder than allowed by synchrotron emission from fast cooling electrons, and roughly half of the GRB population also violate the limit set by slow cooling electrons (e.g., Preece et al. 1998; Kaneko et al. 2006; Goldstein et al. 2012; Burgess et al. 2015; the exact fraction is somewhat dependent on the spectral fitting function used). Second, the observed distribution of the peak energy  $E_{\text{pk}}$  is roughly log-normal, with an FWHM of about one order of magnitude (e.g., Goldstein et al. 2012). There is no a priori reason for synchrotron radiation to produce such a narrow distribution; instead it would be expected to show a broad distribution of  $E_{\text{pk}}$  due to its sensitivity to several parameters—the bulk Lorentz factor of the jet,  $\Gamma$ , the Lorentz factor of accelerated electrons,  $\gamma$ , and the magnetic field strength  $B$  ( $E_{\text{pk}} \propto \Gamma\gamma^2 B$ ). Third, the sharpness of the observed spectral peak appear inconsistent with synchrotron radiation

(Axelsson & Borgonovo 2015; Yu et al. 2015; Vurm & Beloborodov 2016).

Several authors have studied in some detail the first issue—the spectral index at low energies—and suggested ways of hardening the synchrotron spectrum below  $E_{\text{pk}}$  (see Section 7.4 in Kumar & Zhang 2015 for a review of these efforts). For instance, one could assume the synchrotron cooling time to be comparable to the expansion timescale of the jet, so that the electrons are still efficient emitters but in a marginally fast cooling regime. Alternatively, the fast cooling electron spectrum could be modified by a continuous heating process (e.g., Kumar & McMahon 2008; Asano & Terasawa 2009) or by inverse Compton (IC) cooling in the Klein–Nishina range (e.g., Daigne et al. 2011). With favorably chosen parameters, these models could reproduce the average GRB low-energy slope,  $F_\nu \propto \nu^0$ . However, a significant fraction of GRBs would still remain unexplained.

A plausible solution to the puzzle of the GRB spectral shape is provided by the alternative model where the spectral peak is dominated by radiation from the hot photosphere of an *opaque* dissipative jet (see Beloborodov & Mészáros 2017 for a review). Radiative transfer simulations demonstrate that photospheric radiation escapes with a nonthermal spectrum similar to the shape of the observed Band function (Band et al. 1993) (e.g., Pe’er et al. 2006; Beloborodov 2010; Vurm et al. 2011; Giannios 2012). This model naturally explains both the observed range of  $E_{\text{pk}}$  (Beloborodov 2013) and the spectral shape (Vurm & Beloborodov 2016). The hardness of the low-energy spectral index is then limited only by the Rayleigh–Jeans slope of the Planck function, and is consistent with observed values if the jet is moderately magnetized (Vurm et al. 2011) or if the jet has structure on small angular scales (Lundman et al. 2013).

The photospheric model predicts that the MeV peak of the GRB spectrum is mainly shaped by Compton scattering of

<sup>5</sup> Specifically, GRB 041219A (Kalemci et al. 2007; McGlynn et al. 2007; Götz et al. 2009), GRB 061122 (McGlynn et al. 2009; Götz et al. 2013), GRB 100826A (Yonetoku et al. 2011), GRB 110301A, GRB 110721A (Yonetoku et al. 2012), GRB 140206A (Götz et al. 2014).

photons produced below the photosphere. The scattered radiation is intrinsically polarized (Beloborodov 2011), but the polarization of radiation received by a distant observer averages out to zero, as long as the observed outflow can be approximated as spherically symmetric. Thus, the polarization of scattered radiation can only be detected if the symmetry is broken within the patch of the jet visible to the observer, which has an angular size of  $\delta\theta \sim \Gamma^{-1}$ .

Lundman et al. (2014) and Ito et al. (2014) found that polarization degrees of up to  $\Pi \sim 40\%$  can be observed if the jet has significant structure on scales  $\sim \delta\theta$ , particularly if the jet is strongly beamed and its edge falls into the observed patch. Such an orientation is likely if the jet opening angle is not much larger than  $\Gamma^{-1}$ , so that most observers see the jet edge.

The Lorentz factors of GRB jets exceed  $10^2$ , and it is unclear if they can be collimated within angles  $\sim \Gamma^{-1}$ . In this work we consider photospheric emission from jets without significant variations on angular scales  $\delta\theta \sim \Gamma^{-1}$ , which can emit polarized radiation only through the synchrotron mechanism. The magnetic field is assumed to be advected from the central engine by the expanding jet, and its coherency over the transverse angular scale  $\delta\theta \sim \Gamma^{-1}$  is assumed to remain intact throughout the dissipation process. Then the direction of the magnetic field determines the polarization plane.

Vurm & Beloborodov (2016) recently reconstructed the radiative transfer and sub-photospheric dissipation history for several GRBs by fitting simulated spectra to observed spectra. They showed that the jets are heated over a wide range in radius, typically encompassing the jet photosphere. Here we consider the same type of modeling, but we are now interested primarily in the polarization properties of the observed emission. Several versions of the dissipation mechanism have been discussed (Thompson 1994; Eichler & Levinson 2000; Drenkhahn & Spruit 2002; Rees & Mészáros 2005; Beloborodov 2010; Levinson 2012). Our calculations, however, will not be specific to a particular dissipation model. We assume only that a fraction of the dissipated energy is channeled into relativistic electrons and/or positrons, as indicated by observed GRB spectra, and that the rate of dissipation follows a power law in radius. Such nonthermal particles are expected from nuclear collisional dissipation (Beloborodov 2010) or perhaps from (sub-)photospheric internal shocks with significant collisionless subshocks (Beloborodov 2017). Dissipation of magnetic energy through reconnection can also produce high-energy electrons, but its energy budget may be insufficient in the moderately magnetized jets that are preferred by the radiative transfer models of GRB spectra (Vurm & Beloborodov 2016).

The injected relativistic particles emit part of their energy as polarized synchrotron emission. Photons emitted deep below the photosphere, where the scattering optical depth is much larger than unity, will necessarily scatter several times before escaping the outflow and reaching the observer. The original polarization set by the magnetic field is lost in essentially a single scattering, and therefore synchrotron photons produced deep below the photosphere will only contribute to the unpolarized part of the observed radiation. A significant fraction of synchrotron photons produced around and above the photosphere will escape without scattering and preserve their polarization. The relative contribution of these photons to the overall spectrum is a sensitive function of photon energy, as will be demonstrated below.

The goal of this paper is to make quantitative predictions for the expected GRB polarization using recent radiative transfer simulations that reconstruct the contribution of synchrotron emission to GRB spectra. We also explore which of recent bright GRBs would be most promising for the detection of polarization. The paper is organized as follows. We introduce a generic model for the energy dissipation and estimate the qualitative behavior of the energy dependence of the observed polarization degree in Section 2, showing that the keV emission can be strongly polarized if the dissipation extends significantly beyond the photosphere. In Section 3 we perform detailed numerical calculations of the polarization degree as a function of energy for dissipation parameters obtained from spectral fits of three specific GRBs (990123, 090902B, and 110721A), which show that the keV emission of both GRB 990123 and GRB 090902B is expected to have been strongly polarized. Finally, we discuss our results in Section 4.

## 2. Frequency Dependence of the Polarization Degree

At any photon energy  $E = h\nu$ , the observed GRB spectrum  $L_{\text{obs}}(E)$  is the sum of two contributions: photons that escaped the jet after their last Compton scattering,  $L_{\text{sc}}(E)$ , and photons escaping directly after their emission by the synchrotron mechanism, with no scattering,  $L_{\text{nsc}}(E)$ . It is convenient to define the unscattered fraction,

$$f_{\text{nsc}}(E) = \frac{L_{\text{nsc}}(E)}{L_{\text{obs}}(E)}. \quad (1)$$

Then the observed polarization degree is given by

$$\Pi(E) = f_{\text{nsc}}(E)\Pi_{\text{syn}}, \quad (2)$$

where  $\Pi_{\text{syn}}$  is the polarization degree of pure unscattered synchrotron emission. Synchrotron emission from relativistic electrons in a uniform magnetic field  $\mathbf{B}$  is linearly polarized in the plane perpendicular to  $\mathbf{B}$ . The polarization degree for an isotropic electron distribution is  $\Pi_{\text{syn}} = (p + 1)/(p + 7/3)$ , where  $p \equiv -d \ln N / d \ln E_e$  is the slope of the electron spectrum (Rybicki & Lightman 1979). This standard result is somewhat modified when the observed region is a spherical patch in a relativistic outflow carrying an ordered transverse magnetic field (Lyutikov et al. 2003). The polarization degree of optically thin synchrotron emission from relativistic jets has been studied by several authors (e.g., Granot 2003; Granot & Königl 2003; Lyutikov et al. 2003; Nakar et al. 2003; see Lazzati 2006; Toma et al. 2009; Toma 2013 for reviews of GRB models that produce polarized prompt emission). The typical  $\Pi_{\text{syn}}$  varies around 50%. Factors affecting the exact  $\Pi_{\text{syn}}$  have been studied in the previous works and will not be discussed below. In our estimates and figures we will use  $\Pi_{\text{syn}} = 50\%$  as a typical value and focus on  $f_{\text{nsc}}(E)$  as the key factor controlling the observed polarization.

A fluid element within the GRB jet passes through distinct radiative zones as it expands: Planck, Wien, sub-photospheric, and optically thin (Beloborodov 2013). The fate of a synchrotron photon depends on where it is generated:

1. The Planck and Wien zones have a large Compton parameter  $y = 4(k_B T / m_e c^2) \tau \gg 1$ , where  $T$  is the electron temperature,  $k_B$  is the Boltzmann constant,  $m_e$  is the electron mass,  $c$  is the speed of light, and  $\tau$  is the

optical depth to Thomson scattering. The condition  $y \gg 1$  implies saturated Comptonization—any new emitted synchrotron photons that avoid self-absorption and induced downscattering are quickly Comptonized to the Wien peak, reaching kinetic equilibrium with the thermal electrons. The Wien peak at the end of the Wien zone (where  $y$  drops to  $\sim 1$ ) determines the spectral peak  $E_{\text{pk}}$  of the observed GRB (Beloborodov 2013; Vurm & Beloborodov 2016). Using the relation  $E_{\text{pk}} \sim 4\Gamma k_B T$ , one can roughly estimate  $y \sim (\tau/\Gamma)(E_{\text{pk}}/m_e c^2)$ , which shows that the Wien zone ends at  $\tau \sim 10^2$  in a typical GRB.

2. The sub-photospheric zone at  $1 \lesssim \tau \lesssim 10^2$  has  $y \lesssim 1$  and here Comptonization proceeds in an unsaturated regime. Most of the synchrotron photons emitted in this zone do not reach the Wien peak and form the low-energy slope of the GRB spectrum (Vurm & Beloborodov 2016).
3. In the optically thin zone ( $\tau < 1$ ), most of the emitted synchrotron photons will escape without scattering and preserve their initial energy *as well as* polarization state.

The radial dependence of the synchrotron emissivity is controlled by the nonthermal dissipation rate. It is convenient to parameterize the dissipated power per logarithmic interval in radius by

$$\frac{dL_d}{d \ln r} = \epsilon_* L \left( \frac{r}{R_*} \right)^k, \quad (3)$$

where  $R_*$  is the radius of the photosphere (where  $\tau = 1$ ),  $\epsilon_*$  is a parameter describing the strength of the dissipation at the photosphere,  $L$  is the total jet luminosity, and  $k$  is a power-law index that determines where most of the dissipation occurs. The dissipation is assumed to occur in an extended range of radii, including the photosphere. Integration of Equation (3) over the dissipation region gives  $L_d$ , the total luminosity given to relativistic electrons and positrons. It does not include the thermal dissipation channel (which heats the thermal plasma at a comparable or even higher rate) because our interest here is the synchrotron emission from nonthermal particles.

The jet magnetic field is assumed to have been advected from the central engine. In the absence of magnetic energy dissipation and for conical jet expansion, the magnetic luminosity  $L_B$  (the isotropic equivalent of the Poynting flux) is constant with radius, which corresponds to  $B \propto (r\Gamma)^{-1}$ . We parameterize the strength of the magnetic field by the ratio  $\epsilon_B \equiv L_B/L$ . This gives

$$U_B = \frac{\epsilon_B L}{4\pi r^2 \Gamma^2 c}, \quad (4)$$

where  $U_B \equiv B^2/8\pi$  is the energy density of the magnetic field.

Besides the power of nonthermal dissipation, an important parameter is the characteristic Lorentz factor of the injected high-energy particles that dominate the synchrotron emissivity. We denote this Lorentz factor by  $\gamma_0$  (measured in the jet rest frame). Dissipation through nuclear collisions produces particles with the characteristic  $\gamma_0 \sim m_\pi/m_e \sim 300$ , where  $m_\pi$  is the pion rest mass. A moderately relativistic collisionless shock gives post-shock particles with  $\gamma_0 \sim m_p/m_e Z_\pm$ , where  $Z_\pm$  is the self-regulated pair loading factor (Beloborodov 2017). Additional acceleration mechanisms may give electrons with  $\gamma > \gamma_0$ , but their energy budget is significantly smaller and we

will neglect their emission.<sup>6</sup> Our estimates will be normalized to  $\gamma_0 = 300$ . These electrons are in the “fast cooling regime,” i.e., they radiate their energy on a timescale much shorter than the jet expansion timescale.

The emitted synchrotron photons have lab-frame characteristic frequencies  $\nu_0 \approx \Gamma \gamma_0^2 \nu'_B$ , where

$$\nu'_B = \frac{eB}{2\pi m_e c} \propto r^{-1}, \quad (5)$$

is the Larmor frequency,  $e$  is the electron charge, and we denote comoving frequencies with a prime to distinguish them from the unprimed lab-frame frequencies. A key parameter is the characteristic frequency of synchrotron photons emitted at the Thomson scattering photosphere of radius  $R_*$ ,

$$\nu_* \approx \Gamma \gamma_0^2 \frac{eB(R_*)}{2\pi m_e c}, \quad E_* = h\nu_*. \quad (6)$$

The bulk of photons with  $\nu > \nu_*$  are emitted below the photosphere (since  $\nu_0 \propto B \propto r^{-1}$ ), and will be scattered before escaping the jet. However, the bulk of synchrotron photons with  $\nu < \nu_*$  are emitted above the photosphere and will not be scattered, preserving their polarization properties.

The standard expression for the photospheric radius is given by

$$R_* \approx \frac{L \sigma_T Z_\pm}{4\pi m_p c^3 \Gamma^3}, \quad (7)$$

where we took into account the  $e^\pm$  enrichment of dissipative jets by the factor  $Z_\pm$ . The photosphere is quite fuzzy, because the locations of last scattering are broadly distributed around  $R_*$ : 2/3 of photons propagating from large optical depths are last scattered between  $0.3R_*$  and  $3R_*$ , and 1/3 outside this interval (Beloborodov 2011; see also Pe’er 2008). The characteristic lab-frame energy of a synchrotron photon emitted at  $R_*$  is

$$E_* \approx 54 \left( \frac{Z_\pm}{10} \right)^{-1} \left( \frac{\gamma_0}{300} \right)^2 \left( \frac{L}{10^{53} \text{ erg s}^{-1}} \right)^{-1/2} \times \left( \frac{\epsilon_B}{2 \times 10^{-2}} \right)^{1/2} \left( \frac{\Gamma}{500} \right)^3 \text{ keV}, \quad (8)$$

where we have used typical values representative of bright GRBs ( $Z_\pm \sim 10$  was commonly found from the radiative transfer simulations).

As long as the dissipation profile is not too steep (i.e.,  $k < -1/2$ ), the synchrotron emission at frequency  $\nu$  (after integration over all radii where dissipation occurs) peaks at the radius where the characteristic frequency  $\nu_0$  equals  $\nu$ . The simplest estimates for the expected polarization can be made by assuming that all weakly Comptonized synchrotron radiation at frequency  $\nu$  comes from the radius where  $\nu_0 = \nu$ . This approximation is reasonable for synchrotron photons emitted at  $\tau \lesssim 10$ . Then the radial distribution of the synchrotron spectral luminosity is given by

$$\frac{dL_\nu^{\text{syn}}}{d \ln r} \approx \frac{\epsilon_B}{\epsilon_B + \xi_{\text{KN}} \epsilon_{\text{rad}}} \frac{dL_d}{d \ln r} \delta(\nu - \Gamma \gamma_0^2 \nu'_B), \quad (9)$$

<sup>6</sup> The additional particles with  $\gamma > \gamma_0$  could only increase the polarization, so our estimates below will be conservative.



where  $\delta(\dots)$  is the delta function, and the prefactor takes into account that only a fraction of energy given to the nonthermal particles is converted to synchrotron radiation—the rest converts to IC radiation. This fraction is given by  $\epsilon_B/(\epsilon_B + \xi_{\text{KN}} \epsilon_{\text{rad}})$ , where  $\epsilon_{\text{rad}} L$  is the part of the jet power carried by radiation, and  $\xi_{\text{KN}}$  is a factor that takes into account the fact that the IC cooling can be reduced due to the Klein–Nishina reduction of the Compton cross section. As a first approximation,  $\xi_{\text{KN}} \approx (1 + 4\gamma h\nu/m_e c^2)^{-3/2}$ , where  $\gamma$  and  $h\nu$  are characteristic values for the electron Lorentz factor and photon energy, respectively (Moderski et al. 2005). In general, the Klein–Nishina suppression of cooling is quite strong for nonthermally heated GRB jets; if the bulk Lorentz factor is  $\Gamma \gtrsim 300$ , the electron Lorentz factor is  $\gamma \sim 300$ , and the typical observed photon energy is  $\sim 1$  MeV, then  $\gamma h\nu/m_e c^2 \gtrsim 1$ , and  $\xi_{\text{KN}} \lesssim 10^{-1}$ . Synchrotron cooling can therefore compete with IC cooling already at fairly modest values of  $\epsilon_B$ .

Integrating Equation (9) over radius, we obtain the synchrotron spectrum

$$\nu L_\nu^{\text{syn}} \approx \frac{\epsilon_B \epsilon_\star L}{\epsilon_B + \xi_{\text{KN}} \epsilon_{\text{rad}}} \left( \frac{\nu}{\nu_\star} \right)^{-k}. \quad (10)$$

The delta-function approximation is accurate only if the resulting spectrum in Equation (10) is softer than the synchrotron spectrum emitted locally at a given radius by the fast cooling electrons,  $\nu L_\nu^{\text{syn}} \propto \nu^{1/2}$ . Thus one can see that Equation (10) is invalid for steep dissipation profiles with  $k < -1/2$ . In this case the production of synchrotron photons peaks deep below the photosphere at all frequencies, leading to their scattering and suppression of polarization.

The synchrotron emission should be compared with the total GRB emission, which is shaped by both Comptonized photons advected from larger optical depths and locally produced synchrotron photons. The GRB spectrum predicted by radiative transfer simulations shows a transition at low energies from the Comptonized spectrum to the “soft excess” dominated by weakly Comptonized synchrotron radiation. A simple (and crude) estimate for the Comptonized spectrum is a power law with a photon index  $\alpha$ ,

$$\nu L_\nu \approx \epsilon_{\text{rad}} L \left( \frac{\nu}{\nu_{\text{pk}}} \right)^{\alpha+2}, \quad \nu < \nu_{\text{pk}} = \frac{E_{\text{pk}}}{h}. \quad (11)$$

Comparison of Equations (10) and (11) gives an estimate for the frequency  $\nu_{\text{syn}}$  below which the observed emission is dominated by synchrotron emission weakly affected by Comptonization. Equating (10) and (11) one finds

$$\left( \frac{\nu_{\text{syn}}}{\nu_{\text{pk}}} \right)^{\alpha+k+2} \approx \left( \frac{\nu_\star}{\nu_{\text{pk}}} \right)^k \frac{\epsilon_\star \epsilon_B}{\epsilon_{\text{rad}} (\epsilon_B + \xi_{\text{KN}} \epsilon_{\text{rad}})}. \quad (12)$$

For example, GRB 090902B has  $E_{\text{pk}} \approx 2$  MeV and  $\alpha \approx -1/2$ ; the radiative transfer modeling performed by Vurm & Beloborodov (2016) yielded  $k \approx -0.25$ ,  $\epsilon_{\text{rad}} \approx 0.5$ ,  $\epsilon_\star \approx 0.4$ , and  $\epsilon_B \approx 2 \times 10^{-2}$ . Furthermore, the peak energy was high enough for Klein–Nishina suppression of the IC cooling to be significant, with  $\xi_{\text{KN}} \approx 7 \times 10^{-2}$ . This gives  $\nu_{\text{syn}}/\nu_{\text{pk}} \approx 5 \times 10^{-2}$ .

If  $\nu_{\text{syn}} < \nu_\star$ , the synchrotron-dominated part of the spectrum is mainly produced in the optically thin region. Generally, significant observed polarization is expected at frequencies  $\nu \lesssim \min(\nu_{\text{syn}}, \nu_\star)$ . The condition  $\nu < \nu_\star$  implies that the unscattered fraction of synchrotron radiation  $f_{\text{nsc}}^{\text{syn}}(\nu)$  is significant, and the condition  $\nu < \nu_{\text{syn}}$  implies that the spectrum is synchrotron-dominated, so  $f_{\text{nsc}}^{\text{syn}}(\nu)$  defined in Equation (1) is approximately equal to  $f_{\text{nsc}}^{\text{syn}}(\nu)$ . For the parameters of GRB 090902B, both conditions are satisfied for photons of energies  $E \lesssim 200$  keV.

The unscattered fraction of synchrotron emission  $f_{\text{nsc}}^{\text{syn}}$  is a decreasing function of  $\nu/\nu_\star$ , and it is useful to calculate this function using a more detailed synchrotron spectrum of the fast cooling electrons and the accurate probability of photon escape from a given optical depth  $\tau$  without scattering. The calculation is described in Appendices A and B, and the result is (for  $k > -1/2$ )

$$f_{\text{nsc}}^{\text{syn}}(\nu) \approx \left( k + \frac{1}{2} \right) \left( \frac{\nu}{\nu_\star} \right)^{k+1/2} \Gamma \left[ -\left( k + \frac{1}{2} \right), \frac{\nu}{\nu_\star} \right], \quad (13)$$

where  $\Gamma[s, x]$  is the upper incomplete  $\Gamma$ -function (not to be confused with the bulk Lorentz factor). For  $k \sim 0$ , roughly a tenth of the synchrotron photons observed at  $\nu \approx \nu_\star$  have avoided scattering, and so the polarization degree at this frequency is modest. For a much lower frequency  $\nu = 10^{-2} \nu_\star$ , Equation (13) gives  $f_{\text{nsc}}^{\text{syn}} \approx 0.8$ . The polarization degree at such frequencies is almost equal to that of optically thin synchrotron emission.

The unscattered fraction  $f_{\text{nsc}}^{\text{syn}}$  increases with decreasing  $\nu$  because the lower frequency emission is produced at smaller optical depths  $\tau$ —the typical synchrotron frequency  $\nu_0 \propto B \propto r^{-1} \propto \tau$ . If dissipation ends at radius  $R_{\text{end}}$ , the lowest characteristic frequency  $\nu_0$  is  $\nu_{\text{end}} = \nu_\star R_\star / R_{\text{end}}$ . The unscattered fraction will then be largest at  $\nu \lesssim \nu_{\text{end}}$ . For instance, in the model for GRB 090902B, if dissipation occurs up to  $R_{\text{end}} \approx 10^2 R_\star$ , then the corresponding lab-frame energy is  $E_{\text{end}} = E_\star R_\star / R_{\text{end}} \approx 5$  keV.

For even lower photon energies synchrotron self-absorption may become important. The opacity due to synchrotron self-absorption, as a function of radius and comoving frequency, is computed in Appendix C. At  $r = R_{\text{end}}$ , and  $\nu = \nu_{\text{end}} \approx \Gamma \nu'_{\text{end}}$ , the opacity is given by Equation (C3),

$$\tau_{\nu'} \approx \frac{\epsilon_B}{\epsilon_B + \xi_{\text{KN}} \epsilon_{\text{rad}}} \frac{\Gamma \epsilon_\star L}{(4\pi)^2 R_\star^2 \nu_\star^3 \gamma_0 m_e \tau_{\text{end}}^{k+1}}, \quad (14)$$

where  $\tau_{\text{end}} = R_\star / R_{\text{end}}$  is the Thomson scattering optical depth at the outer dissipation radius, and we have assumed that any pair loading of the jet has not significantly affected the  $\tau \propto r^{-1}$  scaling. For the values considered above, we find  $\tau_{\nu'}(R_{\text{end}}) \approx 3 \times 10^{-5}$ , so that absorption does not affect the emission much. However, since  $\tau_{\nu'} \propto \nu^{-3}$  (Equation (C3)), self-absorption will become significant at lower frequencies. On the other hand, at observed energies of  $\lesssim 1$  keV, Galactic absorption is also significant.

### 3. Numerical Models for Three Bright GRBs

The polarization degree  $\Pi(E)$  may be predicted for a detected GRB using its observed spectrum and its numerical model obtained from radiative transfer simulations. The transfer simulations (i) allow one to approximately reconstruct the jet

magnetization and the radial distribution of the nonthermal dissipation rate, which control the synchrotron emissivity, (ii) give the photospheric radius  $R_*$ , and (iii) show the relative contribution of unscattered synchrotron emission  $f_{\text{nsc}}(E)$  to the total observed spectrum (whose peak is dominated by the Comptonized radiation advected from large optical depths).

A significant role is played by  $e^\pm$  pair creation, as it increases  $R_*$  and reduces  $E_*$ . In addition, pair creation affects the synchrotron spectrum produced by the high-energy particles. The standard synchrotron spectrum from fast cooling particles injected with a fixed  $\gamma_0$  is affected by both the competition between synchrotron and IC cooling (with important Klein–Nishina corrections) and the reprocessing of IC radiation into secondary  $e^\pm$  pairs created in the  $e^\pm$  cascade. The cascade can only be suppressed by synchrotron cooling when  $\epsilon_B \gtrsim \xi_{\text{KN}} \epsilon_{\text{rad}}$ . High magnetization therefore increases the polarization degree due to two separate effects: (i) more synchrotron emission is produced, and (ii) the cascade is weaker, so the pair loading and  $R_*$  are reduced, leading to a higher  $E_*$  and opening a broader spectral window  $E < E_*$  for potentially strong polarization. The transfer problem is in general highly nonlinear and requires simulations that self-consistently include  $e^\pm$  creation in photon–photon collisions.

Vurm & Beloborodov (2016) reconstructed the observed spectra of GRBs 990123, 090902B, and 130427A with theoretical spectra obtained by detailed simulations of radiative transfer in a dissipative jet. They used a numerical code that solves the kinetic equations for the electron and photon distribution functions and follows their self-consistent evolution in the expanding jet. The initial version of the kinetic code was designed for static sources (Vurm & Poutanen 2009) and then developed to simulate relativistic jets (Vurm et al. 2011) by solving the radiative transfer equation (Beloborodov 2011). The most recent version of the code (Vurm & Beloborodov 2016) follows the jet evolution from very large optical depths  $\tau \gtrsim 10^3$  and calculates all relevant radiative processes, including synchrotron self-absorption, induced downscattering,  $e^\pm$  creation in photon–photon collisions, double Compton scattering, and bremsstrahlung. The simulations also follow the jet acceleration by radiation pressure.

Here we study two of the previously simulated GRBs, GRB 990123 and GRB 090902B, using the best-fit parameters from Vurm & Beloborodov (2016). For each burst, we identify the unscattered synchrotron component in the emitted spectrum  $L_{\text{nsc}}(E)$  and then find the polarization degree according to Equation (1), where  $L_{\text{obs}}(E)$  is the total spectrum predicted by the transfer simulations. The unscattered synchrotron luminosity is calculated numerically using the known radial dependence of the synchrotron emissivity from the transfer simulations, and the probability for photon escape without scattering (see Appendices A and B).

Additionally, we include GRB 110721A in our sample, a GRB with a claimed detection of prompt emission polarization. Yonetoku et al. (2012) reported a time-integrated polarization degree of  $\Pi = 84^{+16}_{-28}\%$  with a  $3.3\sigma$  confidence level. We first find a radiative transfer model that reproduces the observed spectrum (we used the data from time bin 4, as presented in Axelsson et al. (2012), and assumed a cosmological redshift of  $z = 2$ ). Then we use this model to obtain  $L_{\text{nsc}}(E)$  in the same way as for GRB 990123 and GRB 090902B.

**Table 1**  
Fitted Nonthermal Dissipation Parameters ( $\epsilon_B$ ,  $\epsilon_*$ ,  $\tau_{\text{end}}$ , and  $k$ ) and Derived Characteristic Energies ( $E_{\text{pk}}$  and  $E_*$ ) for GRB 990123, GRB 090902B, and GRB 110721A

Parameter	GRB 990123	GRB 090902B	GRB 110721A
$\epsilon_B$	$1.8 \times 10^{-2}$	$1.1 \times 10^{-2}$	$1.0 \times 10^{-3}$
$\epsilon_*$	$6.8 \times 10^{-3}$	$1.5 \times 10^{-2}$	$2.3 \times 10^{-2}$
$\tau_{\text{end}}$	$1.2 \times 10^{-2}$	$3.0 \times 10^{-2}$	$4.0 \times 10^{-1}$
$k$	−0.19	−0.25	−0.013
$E_{\text{pk}}$ (MeV)	1.4	2.6	1.0
$E_*$ (keV)	69	140	0.88

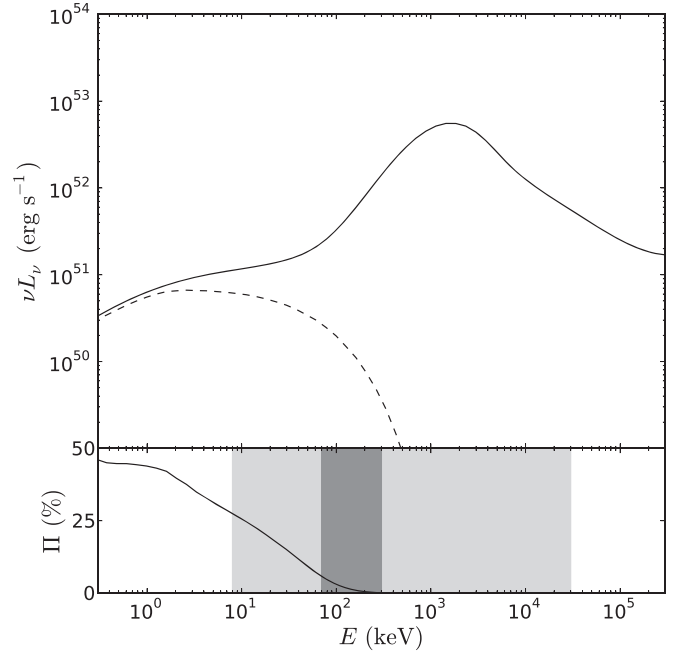


**Figure 1.** Top panel: the simulated GRB spectrum for GRB 990123 (solid line) and the spectrum of unscattered synchrotron emission (dashed line). Bottom panel: the polarization degree (i.e., the ratio of the above spectra times the assumed synchrotron polarization degree of 50%) as a function of energy. The light and dark shaded regions correspond to the energy ranges of *Fermi* GBM (NaI + BGO detectors, 8 keV–30 MeV) and *GAP* (70–300 keV), respectively.

The fitted dissipation parameters of each GRB are listed in Table 1. The table shows only *nonthermal* dissipation parameters (which is the main interest for us here) and omits the thermal heating rate, which was also part of the simulation. For details of the radiative transfer simulations, see Vurm & Beloborodov (2016).

The numerically integrated unscattered synchrotron spectra, as well as the total GRB spectra from the radiative transfer simulations, are shown in Figures 1–3. These figures demonstrate the essential features discussed in Section 2. The MeV peak is unpolarized, because it was formed in regions of large optical depths. Similarly, the spectrum above the peak consists of Comptonized photons that are also unpolarized. Synchrotron emission dominates the spectrum only at low energies, and only a fraction of this emission has avoided scattering before escaping the jet.

In order to observe a significant polarization degree, significant nonthermal dissipation must occur near and above the photosphere. This is the case for GRB 990123 and GRB 090902B (Figures 1 and 2 respectively), which are best modeled by rather flat dissipation profiles ( $k \approx -1/5$  and

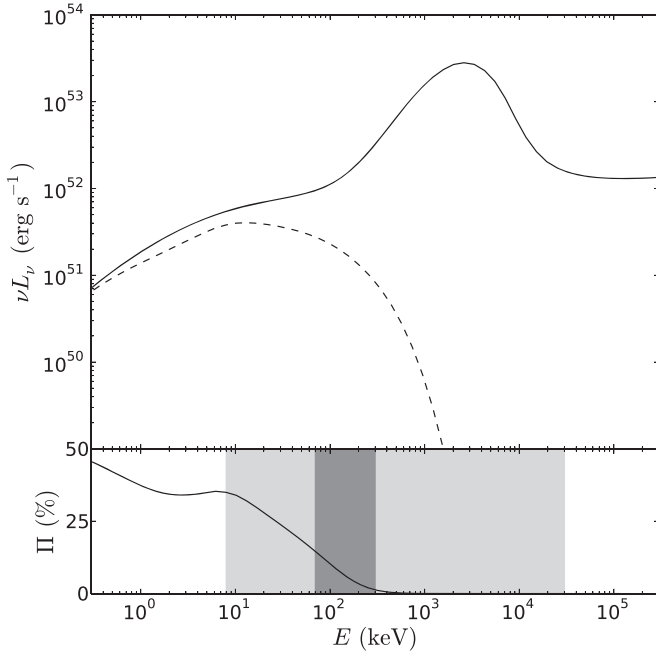


**Figure 2.** Same as Figure 1, but for GRB 090902B.

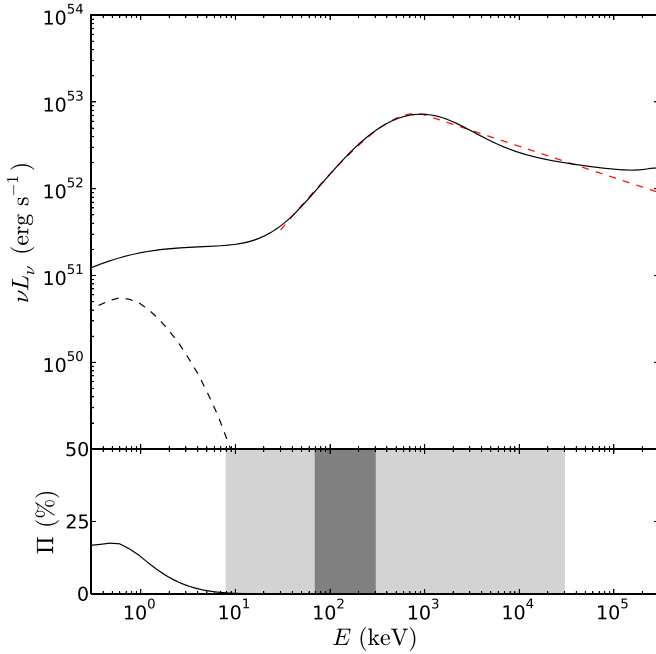


**Figure 3.** Same as Figure 1, but for GRB 110721A. The Band function, which was used for the fit, is shown as a dashed red line.

$k \approx -1/4$ ). The reconstructed properties of these two GRBs are qualitatively similar, resulting in similar spectral features. The reconstructed magnetization,  $\epsilon_B \sim 10^{-2}$ , is strong enough to partially suppress the pair cascade, so that the increase in  $R_*$  due to pair loading is moderate. The partial suppression of the cascade also manifests itself in weaker, less Comptonized high-energy spectra. The full spectra show curvature at  $E \sim E_{\text{syn}} \sim 100$  keV, which coincides with  $E_*$ , indicating the transition to optically thin synchrotron-dominated spectra. At the lowest energies ( $E \lesssim 10$  keV) the spectra curve downwards as a result of synchrotron self-absorption. The observed polarization degrees are a few tens percent at 10–100 keV.

The best spectral fit to GRB 110721A (Figure 3) has an almost flat dissipation profile across the photosphere ( $k \approx 0$ ). The rather weak magnetization  $\epsilon_B \approx 10^{-3}$  results in a fully developed IC  $e^\pm$  cascade. The photosphere was therefore pushed further out, and the characteristic synchrotron energy at the photosphere  $E_*$  was significantly reduced. The resulting polarization degree is significant only at  $E \lesssim 3$  keV.

## 4. Discussion

### 4.1. General Conditions for Polarized Photospheric Emission

The above examples illustrate the conditions leading to significant polarization of GRB emission. First, nonthermal dissipation is required close to the jet photosphere ( $\epsilon_* \gtrsim 10^{-2}$ ), involving injection of nonthermal electrons or positrons. This is expected in GRBs and consistent with their observed spectra (Vurm & Beloborodov 2016). Second, dissipation should not decline too quickly above the photosphere ( $k \gtrsim -1/2$ ), so that synchrotron emission extends into regions of moderate optical depth. Third, the jet must be significantly magnetized ( $\epsilon_B \gtrsim \xi_{\text{KN}} \epsilon_{\text{rad}}$ ) in order to generate a strong synchrotron component. The significant magnetization also weakens the pair cascade, avoiding a dramatic increase in  $R_*$  by pair loading. Under such conditions, polarization degrees of a few tens percent at observed energies of a few tens of keV are expected. Under the most favorable conditions, the upper limit on the polarization degree of our model is about 50%.

Our calculations suggest a relation between the polarization degree  $\Pi(E)$  and the observed spectral shape. The strongest polarization is expected in bursts similar to GRB 090902B, where nonthermal dissipation and the synchrotron component are strong around and above the photosphere. In all of our calculated models, the spectral peak at  $E_{\text{pk}} \sim 1$  MeV is very weakly polarized, because its formation involves multiple scattering below the photosphere, suppressing polarization. This is consistent with the observed sharpness of the MeV peak, which rules out its synchrotron origin (Beloborodov 2013; Axelsson & Borgonovo 2015; Yu et al. 2015; Vurm & Beloborodov 2016).

A detection of strong polarization of the MeV peak would indicate a significant angular structure of the jet. Then the polarized signal must be due to the geometry of the scattering process, independent of magnetic fields or energy dissipation. In particular, strong polarization across the spectral peak is expected when a significant fraction of observed radiation is emitted near the edge of the collimated jet,  $\theta_j$ . The characteristic solid angle occupied by this radiation is  $\Delta\Omega_{\text{edge}} \sim 2\pi[\cos(\theta_j - \Gamma^{-1}) - \cos(\theta_j + \Gamma^{-1})]$ , where we took into account the Doppler beaming of radiation within angle  $\delta\theta \sim \Gamma^{-1}$ . The total solid angle occupied by radiation from all  $\theta < \theta_j$  is  $\Delta\Omega_{\text{tot}} \sim 2\pi[1 - \cos(\theta_j + \Gamma^{-1})]$ , and the probability of observing the edge may be estimated as

$$P_{\text{edge}} \approx \frac{\Delta\Omega_{\text{edge}}}{\Delta\Omega_{\text{tot}}} \sim \frac{4}{\Gamma\theta_j},$$

where  $\cos\theta \approx 1 - \theta^2/2$  has been used. Substituting plausible values of  $\theta_j \sim 0.1$  and  $\Gamma \sim 400$  as an example, one finds that the edge is visible in roughly one tenth of GRBs, so every tenth burst would be strongly polarized. Note, however, that the actual distribution of jet opening angles is uncertain; the existing estimates inferred from so-called “jet breaks” in the light curves of GRB afterglows do not suggest a preferred  $\theta_j$ ,



and in many cases no jet break was detected (see, e.g., Racusin et al. 2009). Polarization studies of the prompt emission above 100 keV could provide a new way to constrain  $\theta_j$ .

Our results demonstrate that in the absence of the edge effects, a moderate polarization is still expected due to the synchrotron component in GRB emission. This polarization can be significant and has the characteristic rise toward soft energies. We note, however, that there is an additional factor that may hinder the detection of synchrotron polarization: its fast variations on unresolved timescales. The radial profile of the jet must be strongly variable, as evidenced by the observed light curves of GRBs, and the magnetic field ejected by the central engine may be strongly variable. For instance, it may alternate on a small radial scale  $\delta r$ , resembling the striped winds from pulsars, and polarization may be measured during a time interval  $\Delta t \gg \delta r/c$ . Such observations can only probe the time-averaged degree of polarization, which could be much smaller than the instantaneous value.

#### 4.2. Comparison to Current Polarization Measurements

To date, observations of GRB polarization have been performed by the *INTEGRAL* and *GAP* satellites. In contrast to *INTEGRAL*, *GAP* was specifically designed and optimized to measure the polarization properties of prompt GRB emission. Both instruments utilize the polarization dependence of the Compton scattering cross section in order to detect a polarized signal. Specifically, photons that first scatter, and then interact with the detector again are registered and used to reconstruct the polarization degree of the incoming signal. By recording the position of both interactions within the detector, and using knowledge of the direction to the GRB, one can reconstruct the distribution of azimuthal scattering angles. The modulation of the distribution is then used to reconstruct the polarization properties of the incoming signal. The requirement of subsequent interactions significantly lowers the effective area of such polarization detectors. The photon statistics are therefore poor in general, with current measurements registering at most a few thousand double events during a GRB. Due to the poor statistics, the polarization measurements are typically time-integrated over the burst duration.

The reported polarization degrees are generally large. The best-fit values appear roughly uniformly distributed between the smallest value of 25% (GRB 100826A, Yonetoku et al. 2011) and the largest value of 84% (GRB 110721A, Yonetoku et al. 2012). The 68% confidence intervals are typically reported to be about  $\pm 20\%$ . We note that measuring the polarization of prompt GRB emission is challenging. As mentioned above, the effective area of the detector is usually small. Non-trivial systematic effects occur due to the fact that the experimental setup is not axially symmetric around the line of sight to the GRB; if not properly accounted for, these effects can mimic the modulation curve of a polarized signal and increase the measurement uncertainty. Furthermore, the polarization degree is a positive-definite quantity. Therefore, the expected value of a measurement will always be larger than zero, also for an unpolarized signal (Weisskopf et al. 2010). Specifically, if  $\Delta\Pi$  is the typical uncertainty of a measurement of polarization degree, then one expects the measured value to be some fraction of  $\Delta\Pi$  of order unity also when the signal is unpolarized:  $\Pi \lesssim \Delta\Pi$ . A better signal-to-noise ratio would be highly desirable in future observations.

It is also difficult to produce such large polarization degrees from a theoretical perspective, especially after averaging over long time intervals, comparable to the burst duration. A confirmation of observed values  $\Pi \gtrsim 60\%$  by future measurements with large signal-to-noise ratios would be truly spectacular and extremely constraining. Polarization degrees of  $\sim 50\%$  could, in principle, be compatible with optically thin synchrotron emission. However, as mentioned in Section 1, optically thin synchrotron emission models struggle to explain the key spectral features of GRBs.

When a realistic photospheric model is used to fit the GRB spectrum, the contribution of unscattered synchrotron emission is found to be small for most bursts. As an example, we considered GRB 110721A. Yonetoku et al. (2012) reported a polarization degree of  $\Pi = 84^{+16}_{-28}$ , with a non-zero detection claimed at a confidence level of  $3.3\sigma$  in the energy range 70–300 keV for the same burst. In contrast, our simulations give a very weak polarization degree in this energy band (Figure 3). Our reconstruction of the spectrum for GRB 110721A, which includes its strong emission at  $E \gg 1$  MeV, suggests a fully developed pair cascade. The cascade increases the number of pairs in the jet and pushes the photosphere to larger radii, where the magnetic field is weaker and synchrotron photons have lower energies,  $E_{\text{syn}} \lesssim 1$  keV. As a result, the simulations predict significant polarization only in the soft X-ray band. We note, however, the limitations of the available spectral fits; a detailed reconstruction of bursts with well measured broadband spectra will be key for accurate polarization predictions.

It is also important to note that detectors using Compton scattering to measure polarization do not weigh the measured polarization degree by photon energy. Each recorded double event carries the same weight for constructing the modulation curve, from which the polarization degree and the position angle are computed. If low-energy photons dominate the observed detector counts, then the measured polarization degree is also dominated by the low-energy photons. This fact should be accounted for when integrating the predicted polarization degree within a specific detector energy range.

C.L. acknowledges the Swedish Research Council for financial support. A.M.B. is supported by NSF grant AST-1412485, NASA grant NNX15AE26G, and a grant from the Simons Foundation (#446228, Andrei Beloborodov).

### Appendix A The Locally Emitted Synchrotron Spectrum

The comoving synchrotron emissivity produced by electrons (and positrons) with a Lorentz factor distribution  $dn_{\pm}/d\gamma$  is given by

$$j'_{\nu'} = \frac{1}{4\pi} \int \frac{dn_{\pm}}{d\gamma} P_{\nu'} d\gamma, \quad (15)$$

where  $P_{\nu'}$  is the spectral power (erg s<sup>-1</sup> Hz<sup>-1</sup>) emitted by each electron, and we have approximated the emissivity as isotropic. We use primes on the comoving emissivity and frequencies to distinguish them from the corresponding unprimed lab-frame quantities.

We will make the simplifying assumption that each electron emits only at its own characteristic synchrotron frequency  $\nu' = \gamma^2 \nu'_B$ , where  $\nu'_B \equiv eB/2\pi m_e c$  is the Larmor frequency.

This gives the spectral power emitted by a single electron in the form  $P_{\nu'} = (\gamma/\gamma_0)^2 P_0 \delta(\nu' - \gamma^2 \nu'_B)$ , where  $\delta(\dots)$  is the delta function and  $P_0 \equiv \gamma_0^2 \sigma_T c B^2 / 6\pi$  is the power emitted by an electron of Lorentz factor  $\gamma_0$ .

The definite relation between the emitted frequency and the electron Lorentz factor simplifies the integral in Equation (15), which gives

$$j'_{\nu'} = \frac{1}{8\pi} \frac{\gamma P_0}{\gamma_0^2 \nu'_B} \frac{dn_{\pm}}{d\gamma}, \quad (16)$$

where  $|d\nu'/d\gamma| = 2\gamma\nu'_B$  was used to integrate out the delta function.

As the outflow propagates a distance  $dr$ , a luminosity  $dL_{\nu}$  (erg s<sup>-1</sup> Hz<sup>-1</sup>) is added to the synchrotron spectrum by the injected relativistic electrons. The luminosity is related to the flux through the sphere of radius  $r$  by  $dL_{\nu} = 4\pi r^2 dF_{\nu}$ , and so we have

$$dL_{\nu} = 4\pi r^2 \int_{2\pi} \mu dI_{\nu} d\Omega, \quad (17)$$

where  $\mu$  is the cosine of the angle to the local radial direction,  $d\Omega$  is a solid angle element, and the integration is over the outer half-sphere (i.e.,  $0 < \mu < 1$ , radiation propagating outwards). The added specific intensity  $dI_{\nu}$  is

$$dI_{\nu} = j_{\nu} \frac{dr}{\mu}, \quad (18)$$

where  $j_{\nu}$  is the lab-frame emissivity. One then finds

$$\frac{dL_{\nu}}{d \ln r} = 4\pi r^3 \int_{2\pi} j_{\nu} d\Omega. \quad (19)$$

The bulk of radiation produced by the jet is radially beamed within angles  $\delta\theta \sim \Gamma^{-1}$ , and this radiation is assumed to have axial symmetry about the radial direction. Integration over the azimuthal angle is then performed by replacing  $d\Omega = 2\pi d\mu$ . The lab-frame frequency is a function of  $\nu'$  and  $\mu$ ;  $\nu = D\nu'$  where  $D \equiv (\Gamma[1 - \beta\mu])^{-1}$  is the Doppler boost and  $\beta$  is the outflow speed in units of the speed of light. Since  $\nu'$  is a function of  $\gamma$ , we may change the variable of integration in Equation (19) to  $\gamma$  for a constant  $\nu$ ,

$$d\Omega = 4\pi \frac{\gamma \nu'_B}{\Gamma \nu} d\gamma. \quad (20)$$

The upper limit of integration is  $\gamma_0$  and corresponds to the lower limit in  $\mu$  (electrons need a larger  $\gamma$  to emit at frequency  $\nu$  if they emit at smaller  $\mu$ ). The lower limit corresponds to electrons emitting radially, as this is the direction of the largest Doppler boost. For the radial direction we have  $\nu = 2\Gamma\nu' = 2\Gamma\gamma_{\min}^2 \nu'_B$ , or  $\gamma_{\min} = (\nu/2\Gamma\nu'_B)^{1/2} = \gamma_0(\nu/\nu_{\max})^{1/2}$ , where

$$\nu_{\max} \equiv 2\Gamma\gamma_0^2 \nu'_B \quad (21)$$

is the highest frequency of emission in the lab frame. The transformation of the emissivity is  $j_{\nu} = D^2 j'_{\nu'}$ , and we have  $\nu = D\nu' = D\gamma^2 \nu'_B$ , so that  $j_{\nu} = j'_{\nu'} (\nu/\gamma^2 \nu'_B)^2$ . Combining Equations (16)–(20) above, we find

$$\nu \frac{dL_{\nu}}{d \ln r} = 4\pi r^3 \frac{2\Gamma\gamma_0^2 P_0 \nu^2}{\nu_{\max}^2} \int_{\gamma_0(\nu/\nu_{\max})^{1/2}}^{\gamma_0} \frac{1}{\gamma^2} \frac{dn_{\pm}}{d\gamma} d\gamma. \quad (22)$$

The unscattered synchrotron spectrum is then

$$\nu L_{\nu, \text{nsc}} = \int \nu \frac{dL_{\nu}}{d \ln r} \exp(-\tau) d \ln r, \quad (23)$$

where  $\tau$  is the sum of the optical depths of Thomson scattering and synchrotron self-absorption. In order to compute the unscattered synchrotron emission spectrum, we numerically integrate Equations (22) and (23), taking  $dn_{\pm}/d\gamma$  and  $\Gamma$  (as functions of radius) from the full radiative transfer simulations.

## Appendix B

### The Approximate Electron Lorentz Factor Distribution

Due to the rapid cooling of the injected electrons (and positrons), the electron Lorentz factor distribution is approximately locally time-independent, and can be found by solving the kinetic equation

$$\frac{d}{d\gamma} \left( \gamma \frac{dn_{\pm}}{d\gamma} \right) + S(\gamma) = 0, \quad (24)$$

or

$$\frac{dn_{\pm}}{d\gamma} = -\frac{1}{\gamma} \int_{\gamma}^{\gamma_0} S(\gamma') d\gamma', \quad (25)$$

where  $S(\gamma)$  is a source term that describes the injection of nonthermal, primary electrons,  $\dot{\gamma} m_e c^2 = -(P_{\text{syn}} + P_{\text{IC}}) = -P_{\text{syn}}(\epsilon_B + \xi_{\text{KN}} \epsilon_{\text{rad}})/\epsilon_B$  describes the cooling of the electron by both synchrotron emission and scatterings, and  $P_{\text{syn}} = (\gamma/\gamma_0)^2 P_0$ . If we assume that all primary electrons are injected at  $\gamma = \gamma_0$ , then  $S = \dot{n}_{\pm}^{\text{inj}} \delta(\gamma - \gamma_0)$ , where  $\dot{n}_{\pm}^{\text{inj}}$  is the injection rate of electrons per volume. Performing the integration in Equation (25), we find

$$\frac{dn_{\pm}}{d\gamma} = \frac{\epsilon_B}{\epsilon_B + \xi_{\text{KN}} \epsilon_{\text{rad}}} \frac{m_e c^2 \gamma_0^2 \dot{n}_{\pm}^{\text{inj}}}{\gamma^2 P_0}. \quad (26)$$

The energy injection rate into the plasma can be written as

$$\dot{Q} = \gamma_0 m_e c^2 \dot{n}_{\pm}^{\text{inj}}, \quad (27)$$

and is related to the dissipated luminosity per logarithmic interval in radius,  $dL_d/d \ln r$ , by

$$\dot{Q} = \frac{1}{4\pi r^3 \Gamma} \frac{dL_d}{d \ln r}. \quad (28)$$

Combining Equations (26)–(28), we find

$$\frac{dn_{\pm}}{d\gamma} = \frac{\epsilon_B}{\epsilon_B + \xi_{\text{KN}} \epsilon_{\text{rad}}} \frac{\gamma_0}{4\pi r^3 \Gamma \gamma^2 P_0} \frac{dL_d}{d \ln r}. \quad (29)$$

Inserting Equation (29) into (22) and integrating over  $\gamma$ , we obtain the locally emitted synchrotron spectrum,

$$\nu \frac{dL_{\nu}}{d \ln r} = \frac{2}{3} \frac{\epsilon_B}{\epsilon_B + \xi_{\text{KN}} \epsilon_{\text{rad}}} \frac{dL_d}{d \ln r} \left( \frac{\nu}{\nu_{\max}} \right)^{1/2} \times \left[ 1 - \left( \frac{\nu}{\nu_{\max}} \right)^{3/2} \right]. \quad (30)$$

This spectrum could also have been obtained by simply considering that the locally emitted spectrum should have  $L_{\nu} \propto \nu^{-1/2}$  due to fast cooling electrons, it should extend up to



$\nu_{\max} \approx \Gamma \nu'_{\text{syn}}(\gamma_0)$ , and the total energy emitted in synchrotron emission is a fraction  $\epsilon_B/(\epsilon_B + \xi_{\text{KN}} \epsilon_{\text{rad}})$  of the total dissipated nonthermal energy (which is obtained by integration of Equation (30) over  $\nu$ ).

### Appendix C

#### Optical Depth due to Synchrotron Self-absorption

The angle-averaged synchrotron self-absorption coefficient is (e.g., Ghisellini & Svensson 1991; Vurm et al. 2011)

$$\kappa_{\nu'} = -\frac{1}{2m_e(\nu')^2} \int \frac{P_{\nu'}}{4\pi} \gamma p \frac{d}{dp} \left( p^{-2} \frac{dn_{\pm}}{dp} \right) dp, \quad (31)$$

where  $p \equiv \beta\gamma$  is the dimensionless electron momentum. For high-energy power-law electrons, which dominate the opacity of synchrotron self-absorption at the frequencies of interest, we have  $p \approx \gamma$ . As above, we approximate the spectral power from a single electron as  $P_{\nu'} \approx (\gamma/\gamma_0)^2 P_0 \delta(\nu' - \gamma^2 \nu'_B)$ , which gives

$$\kappa_{\nu'} \approx -\frac{P_0}{16\pi m_e (\nu'_B)^3 \gamma_0^2} \frac{d}{d\gamma} \left( \gamma^{-2} \frac{dn_{\pm}}{d\gamma} \right). \quad (32)$$

The optical depth of synchrotron self-absorption at a given lab-frame frequency  $\nu \approx \Gamma \gamma^2 \nu'_B$  is then  $\tau_{\nu'} \approx \kappa_{\nu'} r / \Gamma$ . Equation (32) can be evaluated numerically for a given electron Lorentz factor distribution. For estimates, one may use the approximate electron Lorentz factor distribution of Equation (29). Given the dissipation rate of Equation (3) and the approximate electron Lorentz factor distribution, we find

$$\tau_{\nu'} \approx \frac{\epsilon_B}{\epsilon_B + \xi_{\text{KN}} \epsilon_{\text{rad}}} \frac{\epsilon_* L}{(4\pi)^2 r^2 (\nu')^3 \Gamma^2 \gamma_0 m_e} \left( \frac{r}{R_*} \right)^k. \quad (33)$$

### ORCID iDs

Indrek Vurm  <https://orcid.org/0000-0003-1336-4746>

### References

Asano, K., & Terasawa, T. 2009, *ApJ*, **705**, 1714  
 Axelsson, M., Baldini, L., Barbiellini, G., et al. 2012, *ApJL*, **757**, L31  
 Axelsson, M., & Borgonovo, L. 2015, *MNRAS*, **447**, 3150  
 Band, D., Matteson, J., Ford, L., et al. 1993, *ApJ*, **413**, 281

Beloborodov, A. M. 2010, *MNRAS*, **407**, 1033  
 Beloborodov, A. M. 2011, *ApJ*, **737**, 68  
 Beloborodov, A. M. 2013, *ApJ*, **764**, 157  
 Beloborodov, A. M. 2017, *ApJ*, **838**, 125  
 Beloborodov, A. M., & Mészáros, P. 2017, *SSRv*, **207**, 87  
 Burgess, J. M., Ryde, F., & Yu, H.-F. 2015, *MNRAS*, **451**, 1511  
 Daigne, F., Bošnjak, Ž., & Dubus, G. 2011, *A&A*, **526**, A110  
 Deng, W., Zhang, H., Zhang, B., & Li, H. 2016, *ApJL*, **821**, L12  
 Drenkhahn, G., & Spruit, H. C. 2002, *A&A*, **391**, 1141  
 Eichler, D., & Levinson, A. 2000, *ApJ*, **529**, 146  
 Ghisellini, G., & Svensson, R. 1991, *MNRAS*, **252**, 313  
 Giannios, D. 2012, *MNRAS*, **422**, 3092  
 Goldstein, A., Burgess, J. M., Preece, R. D., et al. 2012, *ApJS*, **199**, 19  
 Götz, D., Covino, S., Fernández-Soto, A., Laurent, P., & Bošnjak, Ž. 2013, *MNRAS*, **431**, 3550  
 Götz, D., Laurent, P., Antier, S., et al. 2014, *MNRAS*, **444**, 2776  
 Götz, D., Laurent, P., Lebrun, F., Daigne, F., & Bošnjak, Ž. 2009, *ApJL*, **695**, L208  
 Granot, J. 2003, *ApJL*, **596**, L17  
 Granot, J., & Königl, A. 2003, *ApJL*, **594**, L83  
 Ito, H., Nagataki, S., Matsumoto, J., et al. 2014, *ApJ*, **789**, 159  
 Kalemci, E., Boggs, S. E., Kouveliotou, C., Finger, M., & Baring, M. G. 2007, *ApJS*, **169**, 75  
 Kaneko, Y., Preece, R. D., Briggs, M. S., et al. 2006, *ApJS*, **166**, 298  
 Kumar, P., & McMahon, E. 2008, *MNRAS*, **384**, 33  
 Kumar, P., & Zhang, B. 2015, *PhR*, **561**, 1  
 Lazzati, D. 2006, *NJPh*, **8**, 131  
 Levinson, A. 2012, *ApJ*, **756**, 174  
 Lundman, C., Pe'er, A., & Ryde, F. 2013, *MNRAS*, **428**, 2430  
 Lundman, C., Pe'er, A., & Ryde, F. 2014, *MNRAS*, **440**, 3292  
 Lyutikov, M., Pariev, V. I., & Blandford, R. D. 2003, *ApJ*, **597**, 998  
 McGlynn, S., Clark, D. J., Dean, A. J., et al. 2007, *A&A*, **466**, 895  
 McGlynn, S., Foley, S., McBreen, B., et al. 2009, *A&A*, **499**, 465  
 Moderski, R., Sikora, M., Coppi, P. S., & Aharonian, F. 2005, *MNRAS*, **363**, 954  
 Nakar, E., Piran, T., & Waxman, E. 2003, *JCAP*, **10**, 5  
 Pe'er, A. 2008, *ApJ*, **682**, 463  
 Pe'er, A., Mészáros, P., & Rees, M. J. 2006, *ApJ*, **642**, 995  
 Preece, R. D., Briggs, M. S., Mallozzi, R. S., et al. 1998, *ApJL*, **506**, L23  
 Racusin, J. L., Liang, E. W., Burrows, D. N., et al. 2009, *ApJ*, **698**, 43  
 Rees, M. J., & Mészáros, P. 2005, *ApJ*, **628**, 847  
 Rybicki, G. B., & Lightman, A. P. 1979, *Radiative Processes in Astrophysics* (New York: Wiley)  
 Thompson, C. 1994, *MNRAS*, **270**, 480  
 Toma, K. 2013, arXiv:1308.5733  
 Toma, K., Sakamoto, T., Zhang, B., et al. 2009, *ApJ*, **698**, 1042  
 Vurm, I., & Beloborodov, A. M. 2016, *ApJ*, **831**, 175  
 Vurm, I., Beloborodov, A. M., & Poutanen, J. 2011, *ApJ*, **738**, 77  
 Vurm, I., & Poutanen, J. 2009, *ApJ*, **698**, 293  
 Weisskopf, M. C., Elsner, R. F., & O'Dell, S. L. 2010, *Proc. SPIE*, **7732**, 77320E  
 Yonetoku, D., Murakami, T., Gunji, S., et al. 2011, *ApJL*, **743**, L30  
 Yonetoku, D., Murakami, T., Gunji, S., et al. 2012, *ApJL*, **758**, L1  
 Yu, H.-F., van Eerten, H. J., Greiner, J., et al. 2015, *A&A*, **583**, A129